ZnCohydrotalcite on Ni foam for high-performance supercapacitor

Yubin Yang[1], Shaomin Zhu[2], Hongfeng Xu[3]
[1]School of Materials Science and Engineering, Dalian Jiaotong University, Dalian, P. R. China
[2, 3]School of Environment and Chemical Engineering, Dalian Jiaotong University, Dalian, P. R. China
[2]Corresponding author
E-mail: [1]*ybyang@djtu.edu.cn*, [2]*smzhu@djtu.edu.cn*, [3]*hfx@djtu.edu.cn*

Received 28 December 2022; received in revised form 16 January 2023; accepted 22 January 2023
DOI https://doi.org/10.21595/vp.2023.23142

62nd International Conference on Vibroengineering in Almaty, Kazakhstan, February 10-11, 2023

Abstract. In this paper, hierarchical three-dimensional porous flower of ZnCohydrotalcite non-planar nanosheets were prepared on the surface of Ni foam by in-situ hydrothermal method. Within this material, the foam Ni acted as structural support and nickel sources providing additional active components. This ZnCohydrotalcite demonstrated to have an high specific capacitance reaching 5437.6 mF cm^{-2} at 10 mA cm^{-2} when the ratio of Zn:Co was 2:8 in precursors. Moreover, an asymmetric supercapacitor with obtained ZnCohydrotalcite as anode while activated carbon as cathode exhibited high electrochemical property (30.1 F g^{-1}) and 84.3 % capacitance retention after 20000 cycles at 1 A g^{-1}.

Keywords: supercapacitor, ZnCohydrotalcite, stability.

1. Introduction

In recent years, climate change, oil dependence and other adverse effects have prompted the energy system changes. As a kind of energy storage system, the supercapacitor has built a bridge between the traditional battery and the capacitor [1-3]. Supercapacitor shows high power density, long life, wide temperature range, and environment-friendly, etc. In particular, supercapacitors are the best choice for applications that require simultaneous charge-discharge cycles ranging from seconds to minutes [4-5].

Among different electrode materials for electrochemical capacitors, layered double hydroxides (hydrotalcite), are battery-type electrode materials. It has high specific capacity and energy density due to the reversible Faraday reaction at interface. However, there are still some problems, such as relatively few active sites, easy aggregation during charging and discharging, slow chemical kinetics and so on, which make it difficult to be applied in practice [6-8].

In order to take full advantage of the intrinsic property of hydrotalcite material, we modified the structure of CoAlhydrotalcite by adding zinc, and obtained better electrochemical properties by adjusting the ratio of Zn:Co.

2. Experimental

2.1. Preparation of electrode

Nickel foam pretreatment. The foam nickel was cut to 1×1 cm^2, washed in2 mol L^{-1} hydrochloric acid for 15 min, then washed with anhydrous ethanol and deionized water until the washing water was neutral, and dried at 80 °C for 2-6 h.

Preparation of electrode. All chemical reagents were of analytical grade and no further purification. In typical preparation process, $Zn(NO_3)_2.6H_2O$ (0.04 mmol), $Al(NO_3)_3.6H_2O$ (0.36 mmol), $Co(NO_3)_2.6H_2O$ (0.2 mmol), and $CO(NH_2)_2$ (1.4 mmol) were added into 30 ml deionized water then transferred to 50 ml reactor together with foam Ni. The reactor was in the oven at constant temperature of 120 °C for 10 h. When the temperature was reduced to room

temperature, the nickel foam was removed and washed with deionized water until the washing solution was neutral, dry overnight at 60 °C. The sample is simply recorded as ZnCo-ab, and the values of a and b represent the proportion of Zn and Co in precursor.

Zn-free composite electrode was prepared for comparison by the same process. The sample is recorded as ZnCo-0 (or abbreviated as Co).

2.2. Characterization

Field launch Scanning electron microscope (FE-SEM, Hitachis-4800, Japan) was used to characterization. Acceleration voltage: 0.5~30 kV. X-ray powder diffraction (XRD) analysis of the crystalline composition of material was carried out on PW1710 X-ray diffractometer (Netherlands). Copper Target line was as light source (λ = 1.5432 nm), graphite monochromator (2 kW), hot cathode x-ray tube with tube voltage 35 to 45 kV, and tube current 30 to 40 mA.

Electrochemical properties of the prepared electrodes were measured by electrochemical workstation Chi660e (Shanghai) in 1.0 mol L^{-1}KOH. Typical three-electrode system was used with Pt electrode as the counter electrode, HgO/Hg electrode as the reference electrode, and product as the working electrode. An asymmetric electrochemical capacitor was fabricated by using the prepared electrode as the positive electrode and the activated carbon electrode as the negative electrode. LANHE battery performance test system (Wuhan Blue Electronics Co, Ltd.) was used to test the cycle stability. The test current density is 1 A g^{-1} and the test voltage window is 0 to 1.6 V.

3. Result and discussion

3.1. Physical property analysis of materials

XRD patterns of the as-prepared materials are presented in Fig. 1. Diffraction peaks appeared at 2θ = 11.74, 23.60, 34.69. 39.39, 46.98°, etc. were well attributed to the characteristic diffraction peaks of hexagonal hydrotalcite structure of $Zn_{0.63}Al_{0.37}(OH)_2(CO_3)_{0.185}\cdot\times H_2O$ (PDF 048-1024), corresponding to the crystal planes (003), (006), (012), (015), respectively. In XRD spectra, the characteristic peaks of cobalt oxide or hydroxide were barely monitored, indicating that cobalt element existed in the crystal structure of hydrotalcite. With the increase of Zn: Co ratio in precursor, the peaks in XRD did not shift obviously indicating stable structure of ZnCohydrotalcite. The main peaks (003) and (012) were compared further in Table 1. It was found that the peaks shifted towards smaller angle direction and d value of crystal increased slightly with the increase of Zn: Co ratio. It was speculated that a small amount of Zn(II) doped in the crystal phase by substituting for Co(II) (or Ni(II)) while the substitutions is limited.

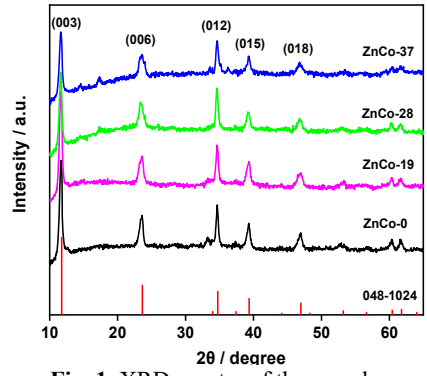

Fig. 1. XRD spectra of the samples

SEM images revealed the morphology difference of products with or without Zn in precursor,

in Fig. 2 and Fig. 3. It can be seen that the ZnCo products (Fig. 2) were distributed in a micron-sized flower cluster, and the petals of each flower cluster were mostly non-planar nanosheets (~30 nm). These nanosheets interconected and formed a three-dimensional structure. Abundant channels and pores in ZnCohydrotalcite were beneficial to electrolyte ions diffusion and migration during electrochemical reaction [9-10].

Table 1. Calculation of d value of ZnCohydrotalcite from XRD characteristics

Sample	(003)		(012)	
	2θ / °	d / Å	2θ / °	d / Å
PDF 048-1024	11.759	7.520	34.729	2.581
ZnCo-0	11.742	7.537	34.690	2.586
ZnCo-19	11.701	7.563	34.644	2.589
ZnCo-28	11.608	7.624	34.636	2.590
ZnCo-37	11.744	7.535	34.642	2.589

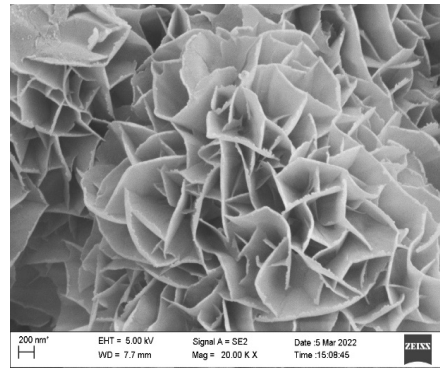

Fig. 2. SEM image of ZnCo-19

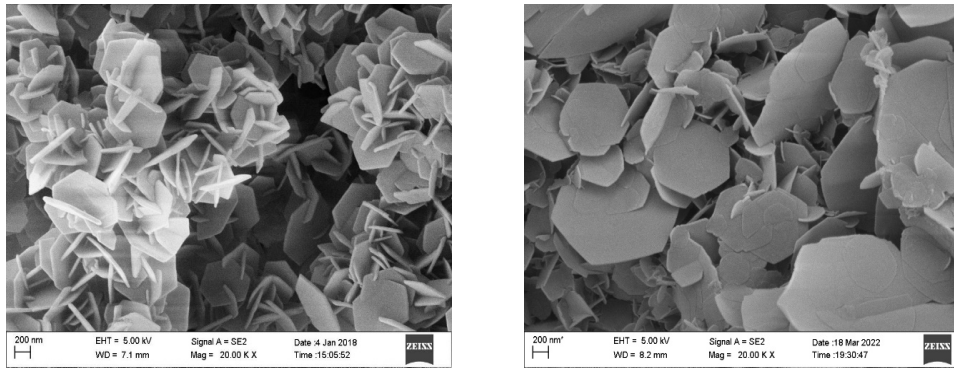

a) b)

Fig. 3. SEM images of the sample with a) Zn and b) Co in precursor

The morphologies of the products with Zn or Co as precursor only were shown in Fig. 3. When Zn was as precursor (Fig. 3(a)), it can be seen that the products on Ni foam were flower-like clusters, where the cluster units interconnected to long chains. The flower sheets were relatively uniform hexagonal two-dimensional sheets with 200-800 nm diameter and 60-80 nm thickness. SEM result of the sample with Co precursor only showed in Fig. 3(b). Most of sheets were regular hexagons with 5 smaller thickness (20-40 nm) and wider granularity distribution from 10 μm to 200 nm. These nanosheets crossed and stacked irregularly to clusters.

By comparison the results above, a significant difference of non-planar sheet units, and defect structure edges could be observed from the morphology of sample with Zn and Co as precursor.

The optimization of microstructure and morphology would influence the electrochemical activity of ZnCo product. The non-planar sheets formed open flower clusters, which structure is beneficial to the effective transport and diffusion of electrolyte ions. On the other hand, it was tested that the crystal composition of products was more inclined to the anisometric compound. There were a lot of defects to balance the charge and then formed more active sites finally. This unique composition and microstructure would lead to relatively high electrochemical activity of ZnCo electrode.

XPS technique was carried out to monitor chemical composition and electronic structure of the samples (Fig. 4). In the spectra of XPS, the characteristic peaks of Zn 2p, Ni 2p, Co 2p, O 1s, Al 2p and C 1s can be observed (Fig. 4(a)). For Co 2p XPS spectra (Fig. 4(b)), the peaks at 797.0 eV and 780.6 eV belonged to the peak superposition of Co 2p1/2 and Co 2p3/2 indexed to Co(II) and Co(III) by fitting [5-6]. In the Ni 2p spectra (Fig. 4(c)), the XPS peaks of Ni 2p1/2 ($Ni(OH)_2$) and Ni 2p3/2 ($Ni(OH)_2$) XPS are observed. In the case of Zn 2p spectra (Fig. 4(d)), the photoelectron peak at 1021.1 eV corresponds to the oxidation state of Zn(II). The peak positions of XPS did not change significantly with increased Zn ratio in precursor, and the peak areas of Co(II) and Ni(II) decreased slightly, showing a decreased content.

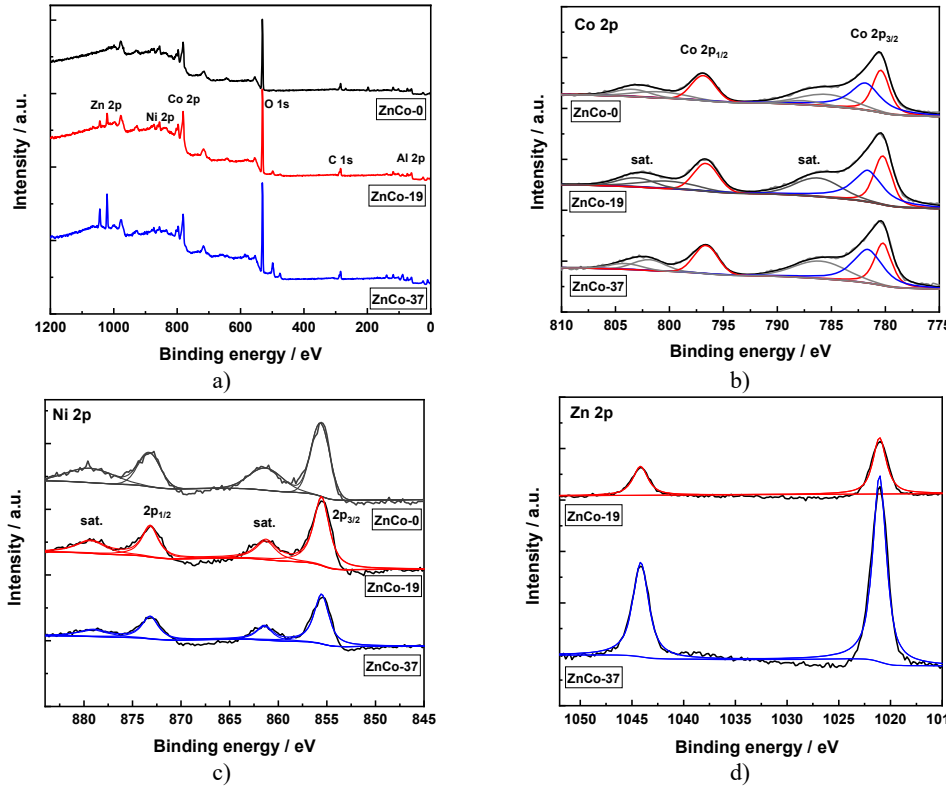

Fig. 4. XPS spectra of the samples, a) survey, b) Co 2p, c) Ni 2p, and d) Zn 2p

3.2. Electrochemical properties analysis

To investigate electrochemical property of ZnCo electrodes, electrochemical tests were carried out. Fig. 5(a) displayed cyclic voltammetry (CV) curves of the as-prepared samples at 10 mV s^{-1}. All curves showed a pair of redox peaks, indicating that the capacitance property of electrode mainly rooted from Faradic redox reaction, reflecting the pseudo-capacitance property [9-10]. Compared with ZnCo-0, ZnCo-19 and ZnCo-28 exhibited relatively higher activity with larger peak current and enclosed area of curves. This higher activity mainly came from more active sites

of smaller particle thickness, size and more defect edges by a certain amount of Zn doping. Moreover, larger crystal plane distance in lattice structure was conducive to ion migration. In galvanostatic charge/discharge (GCD) measurements (Fig. 5(b)), charge-discharge platform can be seen, which again verifies the electrochemical behavior of Faraday electrode.

The areal capacitance value of electrodes can be calculated based on the following equation [11]:

$$C = I \times \frac{t}{S} \times \Delta V, \tag{1}$$

where C was the areal capacitance, Δt (s) and I (mA) represented the discharging time and the present current. ΔV (V) and S (cm^2) were the potential window and the geometrical area of the electrode active materials, respectively.

According to the GCD curves, the calculated areal capacitances are 5325.7, 5420.9, 5437.6 and 4814.4 mF cm^{-2} for ZnCo-0, ZnCo-19, ZnCo-28, ZnCo-37, respectively (10 mA cm^{-2}). ZnCo-19 and ZnCo-28 displayed a higher capacitance values, which was consistent with the results of CV test.

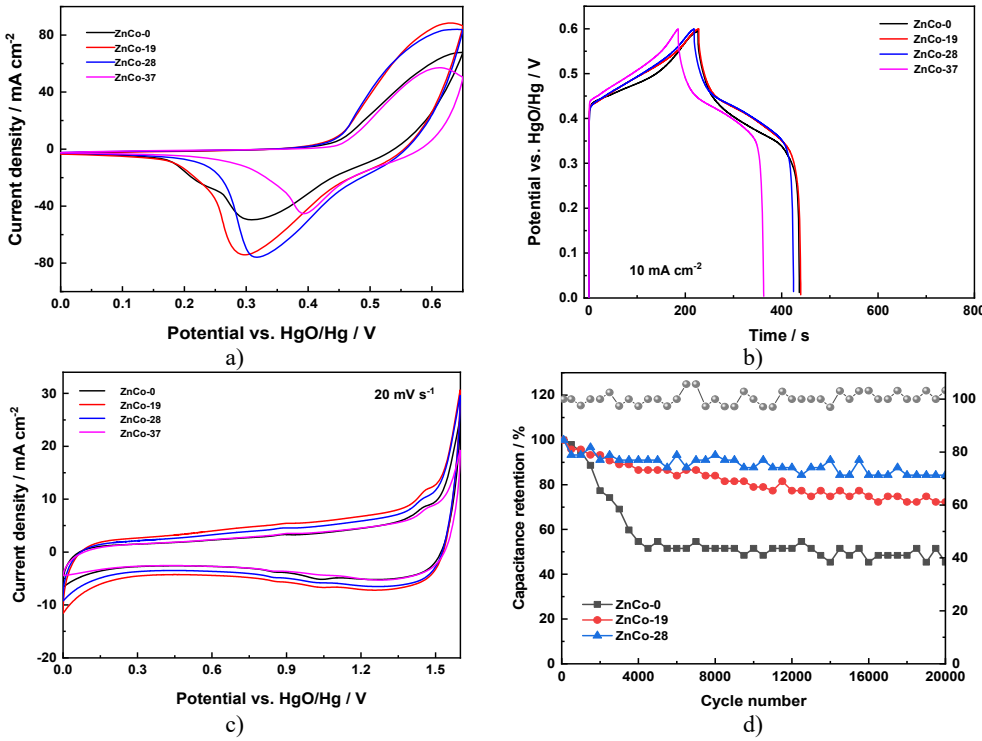

Fig. 5. Electrochemical performance: a) CV curves comparison at 10 mV s^{-1}, b) Galvanostatic charge/discharge curves of electrodes at 10 mA cm^{-2}, c) CV curves of assembled of ZnCo//AC capacitor at 10 mV s^{-1}, and d) ZnCo//AC capacitance retention and columbic efficiency at 1 A g^{-1}

The asymmetric electrochemical capacitor (ZnCo//AC) were assembled to further evaluated the stability of ZnCo electrode. It can be seen that the CV curves is approximately rectangular at 20 mV s^{-1} which showed that the capacitor has good capacitance performance (Fig. 5(c)). The CV curves of ZnCo-19//AC and ZnCo-28//AC exhibited slightly higher response current and curve enclosed area, which were consistent with the test results in the three-electrode system. After 5000 cycles at 1 A g^{-1}, the capacitance retention rates of ZnCo-0//AC, ZnCo-19//AC, ZnCo-28//AC are

54.6 %, 86.6 %, 91.0 %, while after 20000 cycles, the retention rates were 45.4 %, 72.3 % and 84.3 %, respectively (Fig. 5(d)). It can be concluded that a small amount of zinc doping optimized the material microstructure and improved the electrode electrochemical activity and stability.

4. Conclusions

ZnCohydrotalcite composites were prepared on the surface of nickel foam by in situ hydrothermal method with inorganic salts as precursors and nickel foam as matrix. The micro-morphology of ZnCohydrotalcite on foam Ni was a three-dimensional structure by self-assembly of non-planar nanosheets. Zn doping process optimized surface structure and morphology of electrode. The increase of crystal plane spacing and surface defect sites is beneficial to the realization of higher electrochemical performance. The results showed that specific capacitance of ZnCo-28 was 5437.6 mF cm^{-2} (10 mA cm^{-2}). After 20000 cycles, the capacitance retention rate of ZnCo-28//AC was 84.3 %.

Acknowledgements

The authors have not disclosed any funding.

Data availability

The datasets generated during and/or analyzed during the current study are available from the corresponding author on reasonable request.

Conflict of interest

The authors declare that they have no conflict of interest.

References

[1] M. Şahin, F. Blaabjerg, and A. Sangwongwanich, "A comprehensive review on supercapacitor applications and developments," *Energies*, Vol. 15, No. 3, p. 674, Jan. 2022, https://doi.org/10.3390/en15030674

[2] F. Zhang et al., "A high-performance supercapacitor-battery hybrid energy storage device based on graphene-enhanced electrode materials with ultrahigh energy density," *Energy and Environmental Science*, Vol. 6, No. 5, p. 1623, 2013, https://doi.org/10.1039/c3ee40509e

[3] J. Liu, Z. Khanam, S. Ahmed, T. Wang, H. Wang, and S. Song, "Flexible antifreeze Zn-ion hybrid supercapacitor based on gel electrolyte with graphene electrodes," *ACS Applied Materials and Interfaces*, Vol. 13, No. 14, pp. 16454–16468, Apr. 2021, https://doi.org/10.1021/acsami.1c02242

[4] Z. Song, J. Li, J. Hou, H. Hofmann, M. Ouyang, and J. Du, "The battery-supercapacitor hybrid energy storage system in electric vehicle applications: a case study," *Energy*, Vol. 154, pp. 433–441, Jul. 2018, https://doi.org/10.1016/j.energy.2018.04.148

[5] S. Najib and E. Erdem, "Current progress achieved in novel materials for supercapacitor electrodes: mini review," *Nanoscale Advances*, Vol. 1, No. 8, pp. 2817–2827, Aug. 2019, https://doi.org/10.1039/c9na00345b

[6] P. Li, Y. Jiao, S. Yao, L. Wang, and G. Chen, "Dual role of nickel foam in NiCoAl-LDH ensuring high-performance for asymmetric supercapacitors," *New Journal of Chemistry*, Vol. 43, No. 7, pp. 3139–3145, Feb. 2019, https://doi.org/10.1039/c8nj05447a

[7] J. Gou, S. Xie, and C. Liu, "Flower-like Ni-Co hydroxides on Ni foam for high-performance supercapacitor applications," *New Journal of Chemistry*, Vol. 42, No. 6, pp. 4175–4181, 2018, https://doi.org/10.1039/c7nj04663d

[8] W. Cao et al., "Novel fabrication strategy of nanostructured NiCo-LDHs monolithic supercapacitor electrodes via inducing electrochemical in situ growth on etched nickel foams," *Journal of Alloys and Compounds*, Vol. 902, p. 163679, May 2022, https://doi.org/10.1016/j.jallcom.2022.163679

[9] M. Sethi, U. S. Shenoy, and D. K. Bhat, "Hassle-free solvothermal synthesis of NiO nanoflakes for supercapacitor application," *Physica B: Condensed Matter*, Vol. 611, p. 412959, Jun. 2021, https://doi.org/10.1016/j.physb.2021.412959

[10] K. Song et al., "Controlled preparation of Ni(OH)2/NiS nanosheet heterostructure as hybrid supercapacitor electrodes for high electrochemical performance," *Electrochimica Acta*, Vol. 388, p. 138663, Aug. 2021, https://doi.org/10.1016/j.electacta.2021.138663

[11] L. Wang et al., "ZnCo2O4@MnCo2O4 heterojunction structured nanosheets for high-performance supercapacitor," *Journal of Materials Science: Materials in Electronics*, Vol. 29, No. 7, pp. 5782–5790, Apr. 2018, https://doi.org/10.1007/s10854-018-8549-7